

Photo-z for weak lensing tomography from space: the role of optical and near-IR photometry

F. B. Abdalla¹, A. Amara², P. Capak³, E. S. Cypriano¹, O. Lahav¹, J. Rhodes^{3,4}

¹*Department of Physics and Astronomy, University College London, Gower Street, London, WC1E 6BT, UK.*

²*Service d'Astrophysique, CEA Saclay, 91191 Gif sur Yvette, France.*

³*California Institute of Technology, 1201 E California Blvd., Pasadena, CA 91125, USA.*

⁴*Jet Propulsion Laboratory, 4800 Oak Grove Drive, Pasadena, CA 91109, USA.*

8 August 2021

ABSTRACT

We study in detail the photometric redshift requirements needed for tomographic weak gravitational lensing in order to measure accurately the Dark Energy equation of state. In particular, we examine how ground-based photometry (u,g,r,i,z,y) can be complemented by space-based near-infrared (IR) photometry (J,H), e.g. on board the planned DUNE satellite. Using realistic photometric redshift simulations and an artificial neural network photo-z method we evaluate the Figure of Merit for the Dark Energy parameters (w_0, w_a). We consider a DUNE-like broad optical filter supplemented with ground-based multi-band optical data from surveys like the Dark Energy Survey, Pan-STARRS and LSST. We show that the Dark Energy Figure of Merit would improved by a factor of 1.3 to 1.7 if IR filters are added on board DUNE. Furthermore we show that with IR data catastrophic photo-z outliers can be removed effectively. There is an interplay between the choice of filters, the magnitude limits and the removal of outliers. We draw attention to the dependence of the results on the galaxy formation scenarios encoded into the mock galaxies, e.g the galaxy reddening. For example, deep u band data could be as effective as the IR. We also find that about $10^5 - 10^6$ spectroscopic redshifts are needed for calibration of the full survey.

Key words: Cosmology: Photometric redshift surveys – Weak Lensing tomography – Dark Energy

1 INTRODUCTION.

Measuring the nature of Dark Energy has become a central part of current studies in cosmology. A wide number of methods have the potential to probe Dark Energy through its effects on both structure growth and geometry of the Universe (Turner & White 1997; Riess et al. 1998; Perlmutter et al. 1999; Hu 1999; Blake & Glazebrook 2003; Seo & Eisenstein 2003; Hu & Haiman 2003; Blake et al. 2004). Future cosmic shear measurements are now widely believed to have the greatest potential for constraining the Dark Energy equation of state parameter (Peacock & Schneider 2006; Albrecht et al. 2006). However to reach this potential future surveys will require tight control of systematic and statistical errors.

Weak-lensing surveys will have to overcome systematic checks such as a reliable point spread function (PSF) removal, well calibrated shape estimation (e.g. Massey et al. 2006), intrinsic galaxy alignments removal (e.g. King & Schneider 2002, 2003; Heymans & Heavens 2003), shear-shape alignment removal (e.g. Hirata & Seljak 2004; Heymans et al. 2006; Bridle & Abdalla 2007) and pho-

tometric redshifts bias corrections, all of which are vital for the statistical limits of the test to be achieved.

A reliable removal of PSF effects can be greatly improved by using satellite such as the Dark Universe Explorer (DUNE, Réfrégier et al. 2006) or the Supernova/Acceleration Probe (SNAP, Aldering et al. 2004), which will take advantage of the image quality achievable in space to accurately measure the shapes of lensed galaxies. However, obtaining the multiband photometry required to measure photometric redshift from space would require a substantial mission and may not be necessary. In certain wavelengths, obtaining photometry from the ground is much faster and given that a number of large ground based facilities are available and being planned, the case for obtaining photometric redshifts from the ground and shape measurements (and some photometry) from space is compelling.

In this paper we analyse this prospect, with regards to the quality of photometric redshift, for a future project to produce weak lensing measurements with space based data but with a large component of the photometry obtained from the ground. We also assess the impacts on the science goals

arXiv:0705.1437v1 [astro-ph] 10 May 2007

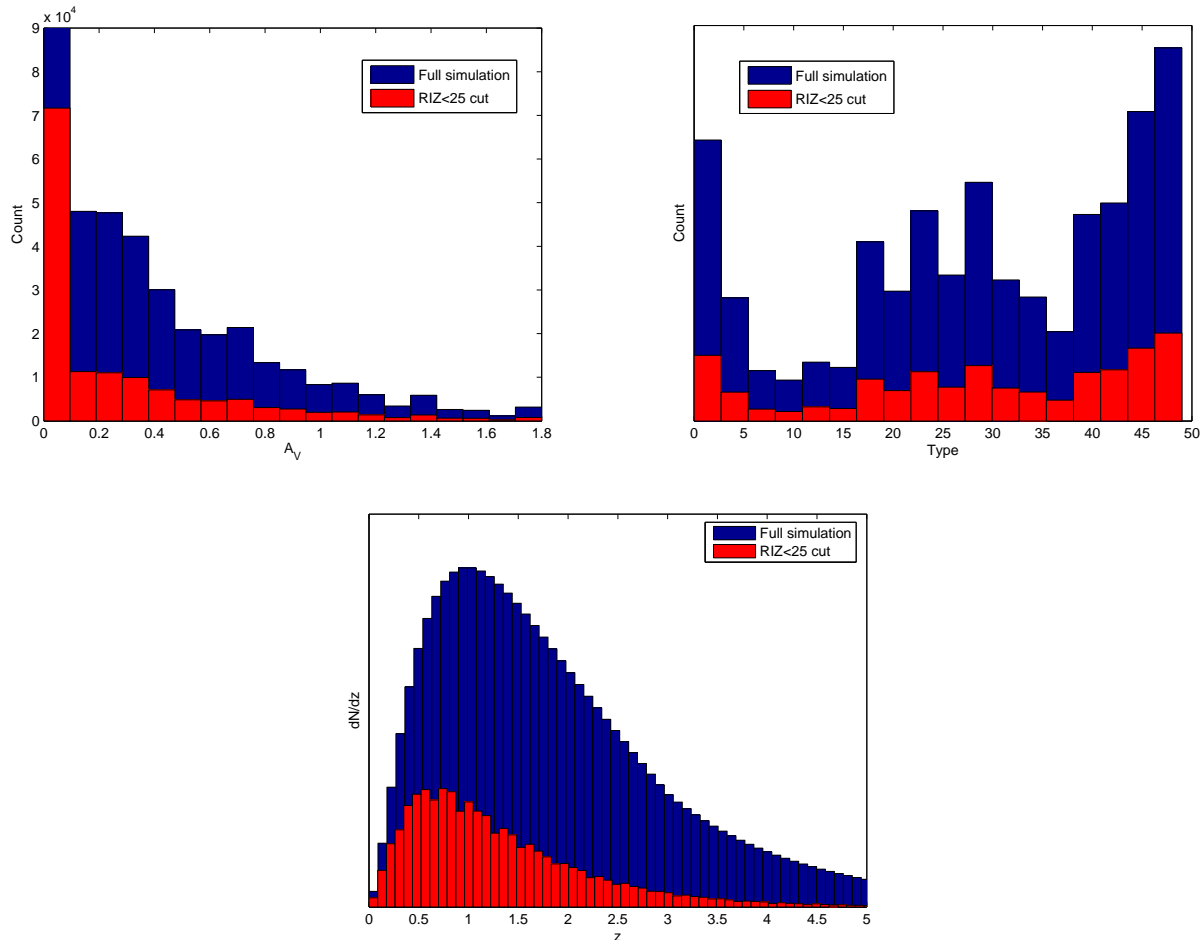


Figure 1. The distributions characterising our simulations. The number density of objects as a function of redshift for the full simulation, which has a magnitude limit of 27, as well as the cut simulations with a magnitude limit in the RIZ band of 25. We also plot the relative number of galaxy types in the simulation with templates numbered from 0 to 50 according to Sec.2, as well as the amount of reddening (A_v) applied to templates in the simulation.

of such a mission given the photometric redshift accuracy. We assess whether the science would benefit significantly by having some photometry from space, especially very red and infrared bands which are difficult to obtain from the ground due to the sky brightness.

We begin by describing the catalogue generation upon which we base our findings. We then make a full photometric redshift analysis with artificial neural networks to assess the accuracy of the photo- z obtained in each of the scenarios considered. We explain the different degeneracies found, their origin and how the different survey bands and depths help in breaking those degeneracies. Finally we translate our photometric redshift errors into a figure of merit for the science considered, in this case for the Dark Energy equation of state derived via weak gravitational lensing tomography.

2 CATALOGUE GENERATION.

In order to simulate the catalogues used in this work, we used the GOODS-N spectroscopic sample from Cowie et al. (2004) and Wirth et al. (2004). This data set includes a

$R < 24.5$ magnitude limited sample along with x-ray, radio, and colour selected objects. The majority of objects are at $z < 1.4$. However, a specific effort was made to include objects at $1.4 < z < 4$. Using these redshifts, we have generated a series of galaxy templates from the broadband photometry, (U,B,V,R,I,Z,J,H,K,HK') using a method similar to Budavári et al. (1999). The key difference is that we assume a prior set of templates (Coleman et al. (1980) (CWW) + Kinney et al. (1996) + intermediate types). We assign the following types to templates: type 0 is Elliptical, type 10 is Sbc, type 20 is Scd, type 30 is Irr, type 40 is SB3 and type 50 is SB2. Intermediate types are a linear interpolation of these types. For instance, type 5 is 0.5El + 0.5Sbc. We, therefore, can remove reddening from the photometry before constructing the templates. Once we have a set of templates, the best fit SED and reddening value for each object is found. We use the Calzetti reddening law (Calzetti 1997). In addition to reddening, we apply a correction for intergalactic absorption by using the Madau law (Madau 1995).

We use the model described below for the luminosity function evolution in the simulation to estimate the RIZ

Band	DES	Pan-4	LSST	Ideal	Ideal + u	DUNE	Cosmos
u	-	-	23.9	-	26.1	-	25.1
g	24.6	25.9	26.1	26.1	26.1	-	25.3
r	24.1	25.6	27.4	26.1	26.1	-	25.3
i	24.3	25.4	26.2	26.2	25.9	-	25.0
z	23.9	23.9	25.1	25.5	25.5	-	24.1
y	-	22.3	24.3	25.0	25.0	-	-
RIZ/F814	-	-	-	-	-	25.0/-	-/25.4
J/B	-	-	-	-	-	23.4/-	-/25.3
H/V	-	-	-	-	-	23.2/-	-/25.2
K	-	-	-	-	-	-	20.2

Table 1. The assumed surveys that we investigate in this work. The values quoted are 10 sigma magnitudes in the AB system. We have taken assumed depths for proposed ground based future imaging surveys and a possible IR survey from space. We also simulate a current ongoing survey over a much smaller area to compare our results.

magnitude and redshift distribution. The RIZ filter is assumed to be a broad filter covering roughly the range 5500 Å to 10000 Å. The local r band luminosity function at $z = 0$ is taken as well as the Steidel et al. (1999) luminosity function at $z = 3$. We linearly interpolate between them in redshift space. At $z > 3$ we assume L^* and the faint end slope are constant, but the volume density which decreases to $10^{-6} h^3 \text{Mpc}^{-3}$ at $z = 10$. We run a Monte-Carlo simulation which draws the RIZ magnitude from this distribution and the reddening and spectral types from the GOODS-N (Cowie et al. 2004) distribution, which should close for a DUNE-like survey since the GOODS spectroscopic limit is $R < 24.5$.

We then calculate fluxes for the galaxy based on the redshift, SED type, and reddening, and filter profiles, normalising to the RIZ magnitude sampled. Finally, we add Gaussian noise to the fluxes, then estimate the magnitudes and errors from the fluxes with noise in the same way as a photometry package would. We plot in Fig.1 the statistical properties of the catalogue, i.e. the galaxy distribution as a function of redshift, reddening and type.

The final catalogue contains galaxies which are complete in the simulation out to a magnitude limit of 27 in RIZ. However given the surveys we are to simulate we cut the catalogue depending on the photometry available. One of the purposes of this study is to assess the impact that space based IR photometry will have on the estimate of Dark Energy parameters. For this purpose we study a fiducial survey which can be achieved by a satellite with a 1.2m mirror. With a 1500s exposure this would reach depths in the IR of around 23 and would reach a depth in optical bands of around 25 in AB and would be feasible with a mission such as DUNE (see Table.1). However this does not restrict our study as it is applicable to any other wide field imager that would provide such data although this is a hard task from the ground. Hence, for an analysis of a DUNE like survey we obtain a cut catalogue which has a 10σ detection in the RIZ filter. Unless we state otherwise we cut the catalogue at an RIZ magnitude of 25. Corresponding photometry is available for other filters obtained from the ground which may be more or less noisy than the RIZ detection. All magnitudes stated in this paper are AB magnitudes.

3 PHOTOMETRIC REDSHIFTS

3.1 Estimating photo- z via neural networks

Essentially there are two approaches to obtain reliable photometric redshifts. Template methods compare the colours found with the photometric data for each galaxy with the colours that templates would predict were these templates placed at different redshifts. Training methods attempt to map out a function which would translate magnitudes to a single photometric redshift. A more detailed description of methods can be found in Csabai et al. (2003) and references within.

It is well studied and accepted that template methods are more versatile and can be applicable when no spectroscopic data is available. However, methods that use training set methods are more reliable and produce better photometric redshifts.

In this work we use artificial neural networks (ANNz), a training set method which has been shown to produce competitive results compared to other training set methods available (Collister & Lahav 2004). ANNz is a supervised neural network training tool. It requires a training set which is the data used to optimise the cost function

$$E = \sum_k (z_{\text{phot}}(\mathbf{c}, \mathbf{m}_k) - z_{\text{train},k})^2, \quad (1)$$

with respect to the free parameters ('weights'), \mathbf{c} , where the sum is over the galaxies in the training set which determines the goodness of fit of the training set. If the data is noisy, a validation set is also required in order to prevent overfitting. This is another portion of the data which also has spectroscopic information available but that is not included in the training process. It is solely used to provide the error function to be minimised.

The remaining freedom left in a neural network analysis is the architecture of the network. A simple architecture is easier to minimise but may not provide the best fit to the data. On the other hand a complicated architecture may remain stuck in a local minimum of the cost function more easily and hence not provide the best solution to the problem either. Here we do not attempt to optimise the architectures for each scenario as we consider that this work does not have as an aim to judge the performance of different photometric redshift techniques. A network with architecture N:2N:2N:1 (i.e. which has N inputs, two hidden

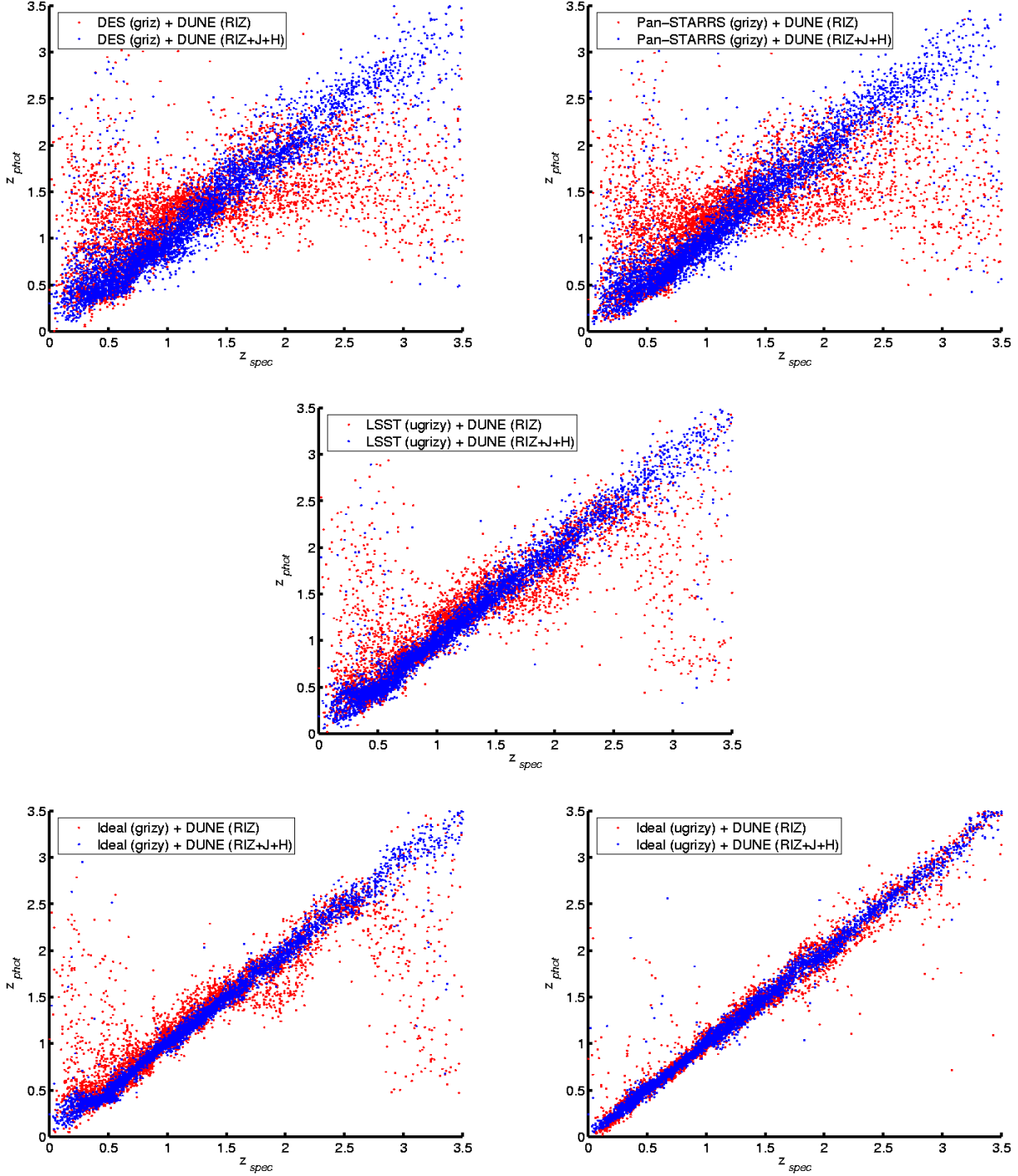


Figure 2. Scatter plots of photometric redshifts as a function of the true redshifts for some of the surveys considered in Sec.3.2. We have shown the galaxies which have photometric and spectroscopic redshifts below 3.5. We have considered optical surveys with increasing depth. The shallowest is a survey with depth similar to DES, followed by a hypothetical survey with depth similar to Pan-STARRS, and finally LSST. We also consider two hypothetical optical surveys with very deep exposures in optical bands, especially in the very red bands, one of which has a very deep u band exposure. We assess in this figure how the inclusion of deep IR data obtained from space would enhance the photometric redshift estimation.

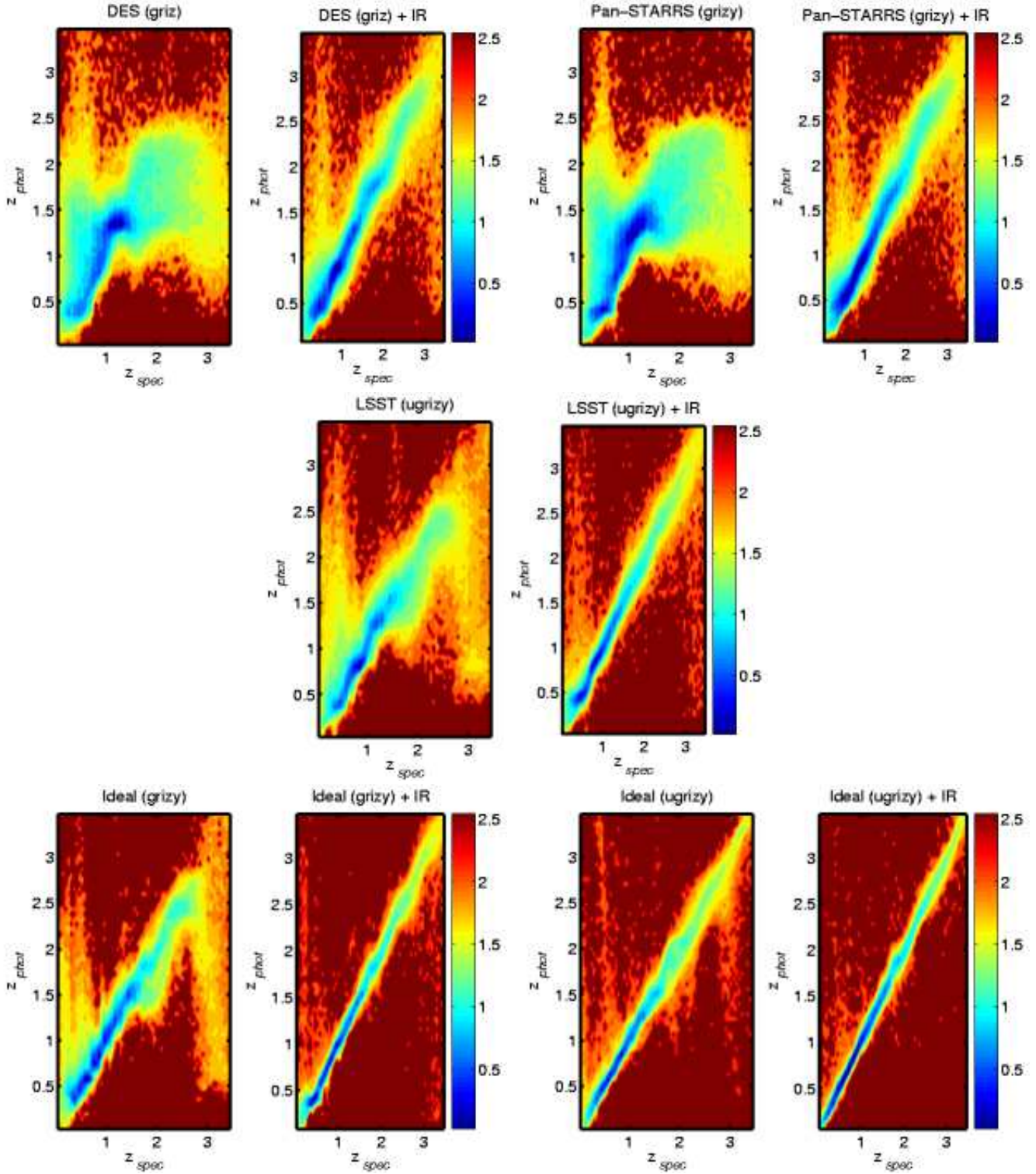


Figure 3. Density maps in the $z_{\text{spec}} - z_{\text{phot}}$ plane. An alternate representation of the data shown in Fig.2. The figures are colour coded according to the local density of points. The colour scheme is exponential; this means that a colour difference which is different by one unit according to the scale means that the density is a factor of $e \simeq 2.718$ smaller. We have shown the galaxies which have photometric and spectroscopic redshifts below 3.5 but the fit has been done over the entire range of galaxies available.

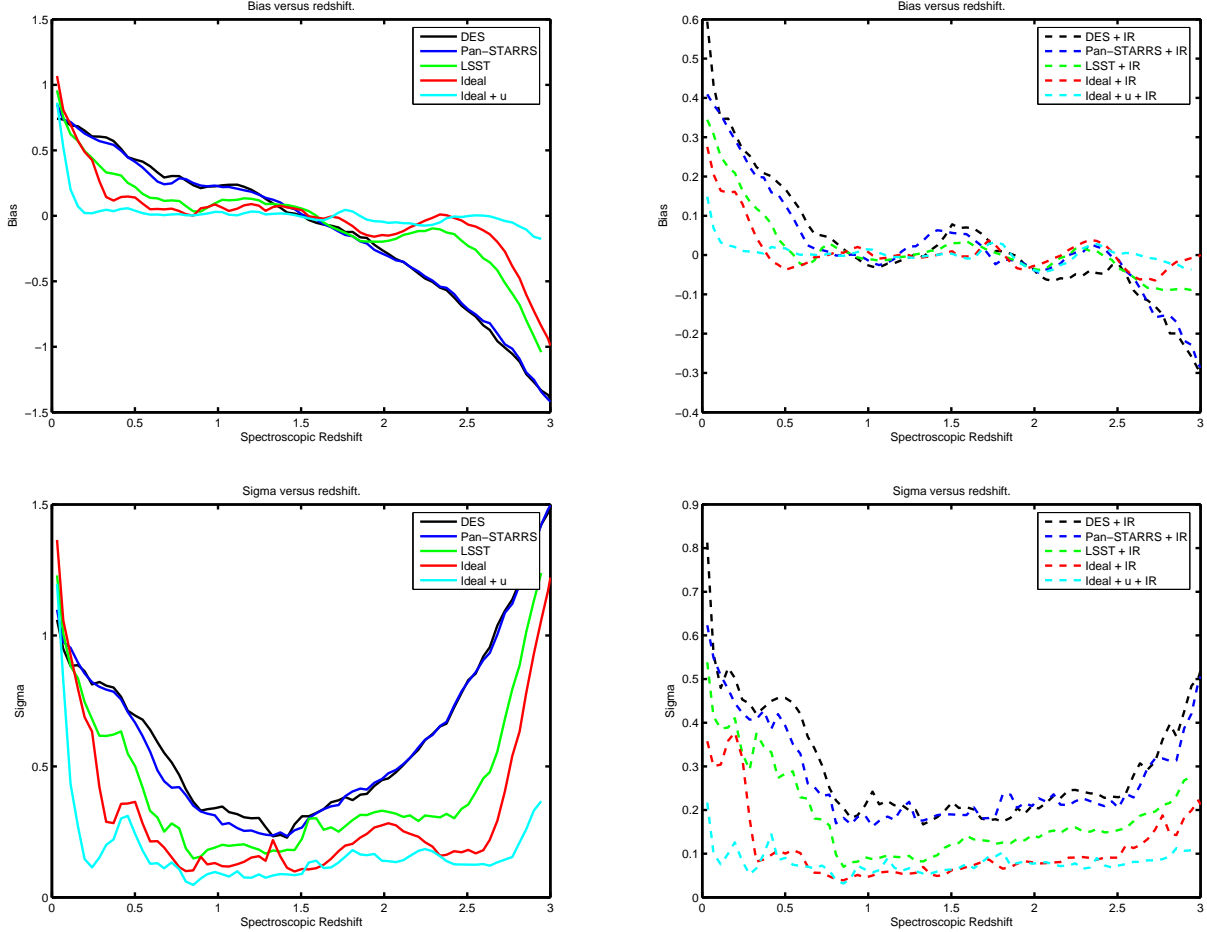


Figure 4. The rms sigma ($\langle(z_{phot} - z_{spec})^2\rangle$, bottom graphs) and the bias ($\langle(z_{phot} - z_{spec})\rangle$, top graphs) as a function of redshift for all the cases considered in this section (left without IR, right including IR). We can see how the inclusion of IR data improves significantly the data with optical exposure times but helps less data with significant optical exposure times although there is still improvement. We can also see the relative importance of bands by comparing surveys with deeper y and z bands and surveys with u band data.

layers with each $2N$ each and only one output estimating the redshift, and where only adjacent layers are interconnected) has been shown to work well on photometric data (Collister & Lahav 2004) where N is the number of different photometric bands available. Therefore we choose this architecture in all our scenarios. For details about the architecture see Collister & Lahav (2004) and references therein.

3.2 Impact of the photometry depth and bands

In this section we compare the results that we obtain on photometric redshifts for different choices of survey depths and different choices of filters for the simulations we have presented in Sec.2. The aim of this section is mainly to assess the impact of the u band, IR bands and the redder optical bands (z and y) on the output of a photometric redshift code.

We have chosen five optical baseline surveys. One which has a depth equivalent to what the Dark Energy Survey (DES) will be able to provide, roughly going down to a magnitude limit of 24 in the for bands (griz); another is an equivalent to what the collection of four Pan-STARRS tele-

scopes will provide, potentially obtaining an order of magnitude increase in depth in the five bands (grizy); the third is an estimated what an optical survey with a Large Synaptic Survey Telescope (LSST) would achieve, obtaining another order of magnitude increase in depth in 6 bands (ugrizy). We have also considered two ideal optical surveys, one without u band photometry but which a very deep exposure on the z and y bands; another which is very similar to the first but with very deep u band imaging. The depths of these surveys are outlined in Table.1 and are chosen to be roughly consistent with the limits which the Dark Energy Survey¹ (which will survey the sky with the 4m Blanco telescope), Pan-STARRS 4² (which will be a collection of four 2m telescopes) and LSST³ (a project to survey the sky every night with a large 8m telescope) will be able to attain although the conclusions of this study are not dependent on particulars of these projects.

We measure photometric redshifts with these baseline

¹ <http://decam.fnal.gov>

² <http://pan-starrs.ifa.hawaii.edu>

³ <http://www.lsst.org>

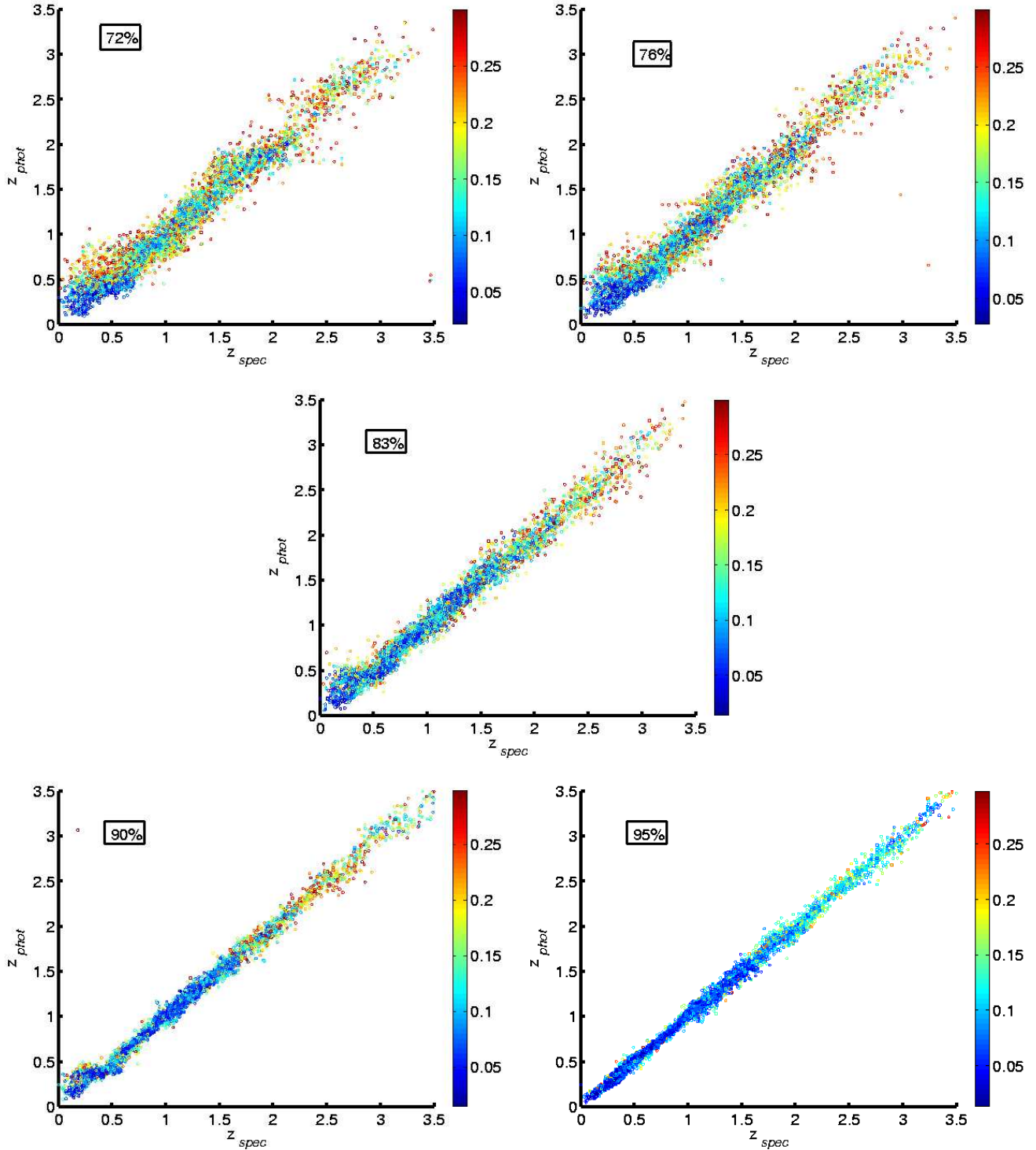


Figure 5. Cleaned catalogues for the 5 surveys considered before. All surveys contain IR information. As explained in Sec.3.3, we have removed all photometric redshifts with an error estimate larger than 0.3. After a neural network is trained it can assess the error on the photometric redshift looking at the error in in the photometry, this value is used for the cut presented here. We can see from all the scatter plots that although the error estimate from the neural networks is not the best available it is able to remove the correct galaxies and provide correct photo-z for some of the sample. After the cut, only 72% of the galaxies were left on the DES+ IR catalogue; 76% had good photo-z on the Pan-STARRS + IR catalogue; 82% of the sample on the LSST + IR catalogue; 90% and 95% of the sample on the Ideal + IR and Ideal + u + IR catalogues respectively. As we can see from Fig.6 a clipping of 0.3 is indeed conservative, we can clean the different catalogues at a higher error estimate but we make a comparison between catalogues here. We stress that this is not a sigma clipping, we do not use information about the spectroscopic redshift of the sample to make this cleaning procedure, we only use the photometry.

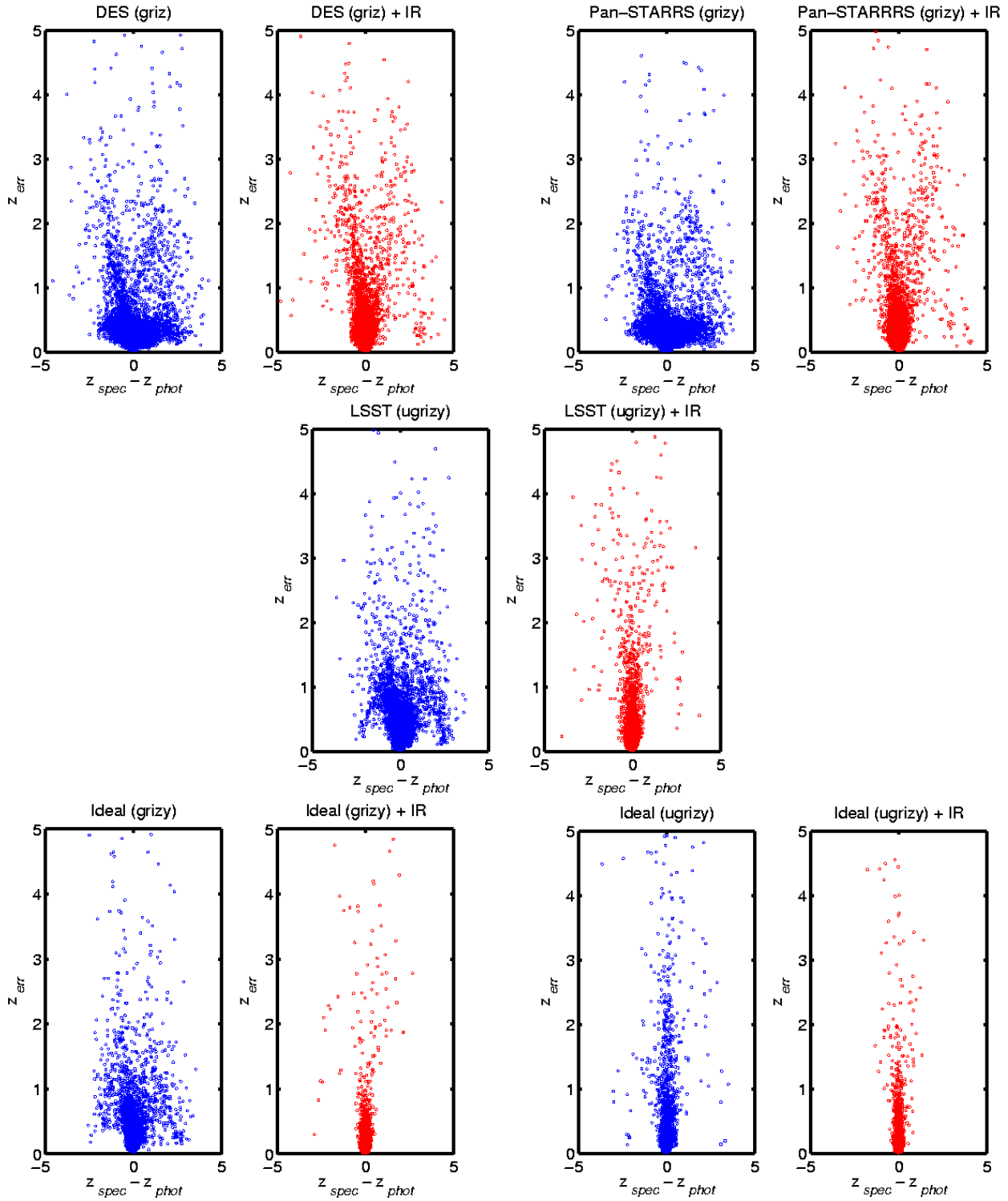


Figure 6. The relation between $z_{phot} - z_{spec}$ as a function of the error predicted by the neural network z_{err} based on the errors from photometry. We can clearly see that the error estimate becomes more reliable the deeper the survey is. Furthermore, the error estimate is more reliable when IR data is obtained. We also note that in the specific case of neural network error estimates, with IR data the error is somewhat overestimated. These scatter plots show that in the case of DES + IR a cut at 0.3 is appropriate to remove most outliers.

Survey - σ	$0 < z < 1.5$	$1.5 < z < 3$	$0 < z < 3$
<i>Des</i>	0.545	0.636	0.572
<i>Des + IR</i>	0.330	0.238	0.307
<i>Pan</i>	0.515	0.635	0.552
<i>Pan + IR</i>	0.289	0.233	0.274
<i>LSST</i>	0.392	0.429	0.403
<i>LSST + IR</i>	0.211	0.155	0.197
<i>Ideal</i>	0.296	0.310	0.300
<i>Ideal + IR</i>	0.119	0.097	0.113
<i>Ideal + u</i>	0.170	0.160	0.167
<i>Ideal + u + IR</i>	0.074	0.080	0.076
Survey - σ_{68}	$0 < z < 1.5$	$1.5 < z < 3$	$0 < z < 3$
<i>Des</i>	0.346	0.559	0.412
<i>Des + IR</i>	0.147	0.175	0.155
<i>Pan</i>	0.327	0.548	0.391
<i>Pan + IR</i>	0.128	0.166	0.139
<i>LSST</i>	0.167	0.276	0.196
<i>LSST + IR</i>	0.085	0.119	0.094
<i>Ideal</i>	0.122	0.173	0.136
<i>Ideal + IR</i>	0.047	0.075	0.054
<i>Ideal + u</i>	0.052	0.122	0.067
<i>Ideal + u + IR</i>	0.036	0.063	0.043

Table 2. The σ_{68} (defined by the interval in which 68 per cent of the galaxies that have smallest $z_{phot} - z_{spec}$ lie within) and σ (defined by $\langle (z_{phot} - z_{spec})^2 \rangle$) for different choices of depths and filters. A comparison of these two numbers assesses how many outliers there are on the sample and whether the distribution of photometric redshifts for a given spectroscopic redshift interval is Gaussian or has broad tails. We note that in order to obtain reliable photo- z for galaxies with an RIZ depth of 25, shallower surveys such as DES or Pan-STARRS are not well matched to DUNE, hence the scatter is large. We note that shallower surveys would not use such faint galaxies for lensing. Deeper optical surveys are necessary to reproduce good photo- z on a galaxy-by-galaxy basis, however IR data considerably improves even the shallower surveys.

surveys both including and excluding the additional information that a space based mission would add with infrared detectors. We plot our findings in Fig.2 and Fig.3 and show the scatter in redshift intervals in Table.2 and Fig.4. The sigma is the r.m.s. photometric redshift error around the mean, and σ_{68} , the interval in which 68 per cent of the galaxies have the smallest value of $z_{spec} - z_{phot}$. We can see from the blue samples of Fig.2 how the increasing depth of the optical survey is significant in obtaining photometric redshifts. We find that to obtain reliable photometric redshifts for a sample with an RIZ magnitude below 25 we are still improving significantly the quality of the photometric redshifts if the overall photometry is as deep as 26 or larger. We note that in order to obtain reliable photo- z for galaxies with an RIZ depth of 25 shallower surveys such as DES or Pan-STARRS are not well matched to DUNE, deeper surveys are necessary to reproduce good photo- z on a galaxy-by-galaxy basis, however IR data considerably improves even the shallower surveys.

We can also see, by analysing these scatter plots, the relative importance of different bands. We can assess, for instance, how much the deeper exposure times in the z and y bands would help in producing reliable photometric redshifts compared to near infrared data; if we compare the LSST + IR case with the ideal case without u band we can

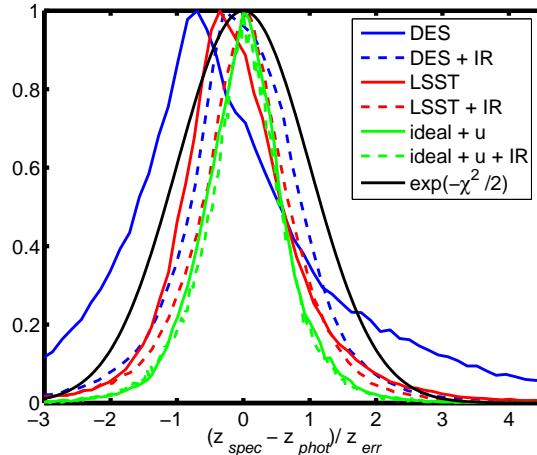


Figure 7. Fit to the unnormalised histograms of the quantity $(z_{spec} - z_{phot})/z_{err}$. If the error estimator is reliable, the quantity above being one corresponds to the one sigma error limit. Therefore 68% of the points should have $(z_{spec} - z_{phot})/z_{err}$ smaller than one in absolute value and centred around zero. We plot this fit for six cases described in Sec.3.2 with and without IR data. We can see that for a cut in RIZ at magnitude 25, the shallower surveys produce data which leads to an biased error estimate with neural networks. All cases with IR data have a much better error estimate and therefore cleaning can be done more efficiently. We can see that the error estimates are less biased with the LSST case at this depth and are not biased at all if we have deeper u, z and y data optically. We also plot the curve $exp(-x^2/2)$ for comparison. If the photo- z error estimate is reliable, then the distributions shown here should be close to Gaussian. We can see for instance that the blue curve does not have very reliable photo- z error estimates whereas the curves with IR data do have more reliable error estimates.

see that out to redshift $z \sim 1.6 - 1.7$ the deeper z and y bands help and the improvement due to IR data is not as large as when the depths in y and z are shallower, however for photometric redshifts of galaxies above a redshift of $z \sim 2.5$ are only improved by the inclusion of IR data. We can understand this behaviour of the error in the photometric redshift estimate with the following argument: most of the information in photometric redshifts come from the 4000 Å break in galaxy spectra, hence the best photometric redshift estimates are expected at the redshifts where the 4000 Å break fall between bands with deep exposures. We can see that optical surveys have best photometric redshift estimates around a redshift of $z \sim 0.7$ which corresponds to the 4000 Å break falling in the i band, hence having measurements of the spectrum on both sides of the break. Similarly, galaxies at a higher redshift are helped by the measurement of the break redshifted into the IR bands. This argument also applied to the Lyman break which occurs at 912 Å. This break is redshifted to the blue part of the spectrum for galaxies around redshift $z \sim 2 - 2.5$, hence u band data also helps photometric redshifts for galaxies in this region of the spectrum.

The addition of u band data can help significantly the photometric redshift determination of certain galaxies. This information is helpful to remove catastrophic outliers that have a small redshift spectroscopically and which have relative flat SEDs. We can see, comparing LSST and DES or

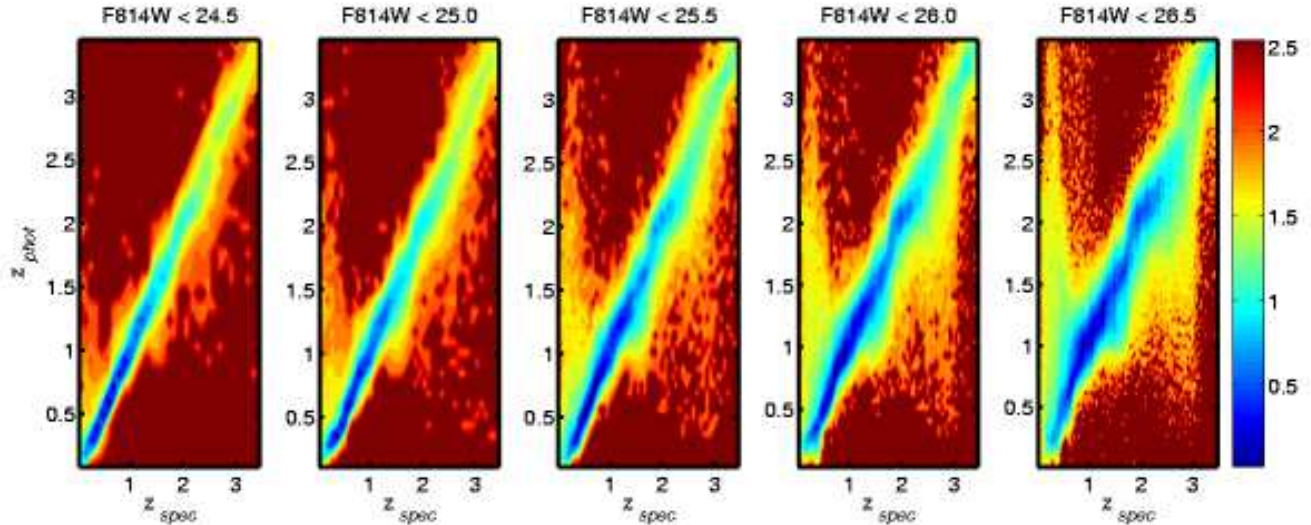


Figure 8. Density plots in the $z_{phot} - z_{spec}$ plane for increasing depth of a catalogue. We have taken mock catalogues from the derived from the Cosmos survey and we have made cuts in the filter F814W at several magnitude cuts from 24.5 to 26.5 in steps of 0.5 in magnitude. We have assumed complete training sets with the same number density of training galaxies per colour volume for every case shown here. as we can see the bright galaxies with high signal to noise have well constrained photometric redshifts whereas the noisy galaxies have almost unconstrained photometric redshifts. The plots are colour coded and the scale is exponential; a colour difference corresponding to one is equivalent to the density being decreased by a factor of e .

Pan-STARRS, that there are indeed fewer outliers if we include u band imaging to our mock survey. However, comparing the LSST simulated results with the idealised survey including a much deeper u band imaging we see that the u band depth has to be larger than 24 if we want all the catastrophic outliers to be removed for a RIZ survey below 25; indeed at a magnitude limit for the u band of 26 almost all the catastrophic outliers have been removed. We note that these integrations on the u band are extremely hard verging on the impossible even with next generation surveys. We also note that the inclusion of u band data has similar effect as the inclusion of IR data in the case of an idealised survey; the scatter including IR data is still significantly improved (see Table.2 and Fig.4), but there are not many outliers with optical data only.

We have also assessed in Table.2, to what extent there are outliers in our analysis depending on the bands. We have calculated σ as well as σ_{68} for each simulation. Whereas the standard deviation gives us the spread for the entire sample, σ_{68} does so only for 68% of the galaxies which have best photometric redshifts. Hence σ_{68} is insensitive to outliers whereas σ is very sensitive to them.

3.3 Cleaned catalogues

When a neural network is trained, we may obtain an estimate for the error on each of the photometric redshifts predicted. This error is obtained the following way. For every scenario, the inputs of a neural network have an associated noise to them. We can assess the variance that this noise would introduce into the output of the network by changing variables from the variance in output with respect to the weights into the variance of the inputs via the formula

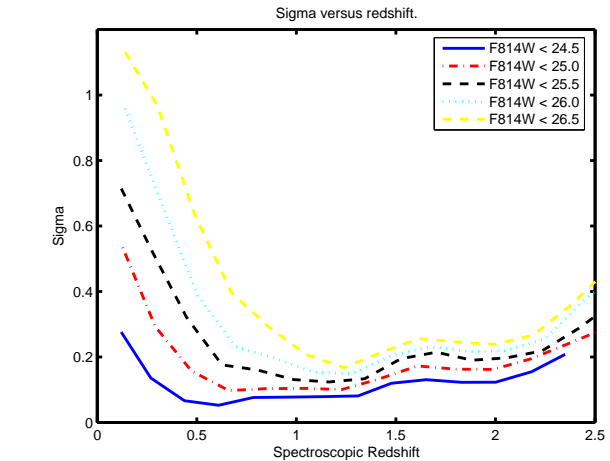


Figure 9. The rms scatter of $(z_{phot} - z_{spec})$ as a function of redshift for samples with different magnitude cuts. Same data as in Fig.8. As we can see brighter samples have less galaxies but also have much better photometric redshifts with many less outliers and smaller scatter.

$$\sigma_z^2 = \sum_i \left(\frac{\partial z}{\partial m_i} \right)^2 \sigma_{m_i}^2 \quad (2)$$

where the sum over i is a sum over all the network inputs.

In order to obtain the quantity $\partial z / \partial m_i$ we can use an algorithm using the activation function for the weights of the network described in (Bishop 1995). This algorithm is fully incorporated in the package ANNz (Collister & Lahav 2004) which we use here.

We have plotted in Fig.5 the IR catalogues cleaned conservatively at a photometric error estimate of 0.2. We have chosen this level of cut as it removes a large majority of the

outliers in the shallower catalogue (DES + IR). In this case we can see that around 40% of the sample has been removed from the data however the quality of the photometric redshifts is almost free of catastrophic outliers. We can see that retaining this conservative cut, the fraction of galaxies which is included into the cut increases according to the depth of the optical plus IR survey. For the ideal + u + IR case only 7% of galaxies are cut and there are no outliers.

We also plot in Fig.6 a scatter diagram for 20000 galaxies representing the errors estimate by the neural network as a function of the difference between the photometric and spectroscopic redshifts. This shows us the reliability of the error estimate. We can see that the error estimate is relatively good if there is IR data included whereas it is not optimal with optical data only; the points with low photometric redshift error are concentrated around $z_{spec} - z_{phot} \sim 0$ for optical plus IR data but not if we have optical data only. In fact when IR data is included the error estimate overestimates the real error in the sample. We find that for optical data only, the deeper surveys can be cleaned by removing the higher error galaxies, however this becomes harder to do with the shallower surveys. This is mainly because the magnitude cuts for the sample have been done here at RIZ of 25 and the shallower surveys have such large scatters; the large scatters are dominated by the fainter sources and this biases the error estimation.

In order to assess whether bands are necessary to obtain good photometric redshift error estimates with neural networks and be able to clean the catalogues efficiently we have plotted in Fig.7 the unnormalised histograms of the quantity $(z_{spec} - z_{phot})/z_{err}$. Each galaxy in the mock will have such ratio; if the error estimate is reliable then the shape of the histogram for this quantity should be centred around zero and there should be roughly 68% of galaxies with $(z_{spec} - z_{phot})/z_{err} < 1$, in absolute value. We can see in Fig.7 that the shallower optical survey is not able to produce data good enough to produce reliable photometric redshift errors at a magnitude cut at RIZ of 25. In fact it is the range of wavelengths probed that produce a more reliable photometric redshift error estimate; i.e. by including IR data the improvement is great, however by including u data or z and y data it is also possible to obtain good photometric redshift errors and clean the catalogues as shown previously.

3.4 Impact of the source catalogue depth

In a catalogue generation we should always define a certain cut where we define what an object is. We have taken in this paper a magnitude cut in a given band to define our catalogues. Here we will show who this cut influences the quality of the photometric redshifts and the photometric redshift errors that are associated to each catalogue. The larger the photometric signal to noise ratio, the better any code will be able to recover a photometric redshift for that galaxy. Therefore we can obtain very deep photometry and produce a catalogue of brighter objects which will have better photometric redshifts and associated photometric redshift errors or have a catalogue of fainter sources where the photometric redshifts and their associated errors are less reliable.

We plot in Fig.8 the results where we have used the simulated survey similar to the COSMOS survey as described in Tab.1. We have used in each subplot only a subset of the

entire set of galaxies we have simulated. The cut was done on the F814W filter, with depths of 24.5, 25, 25.5, 26 and 26.5. As we can see the bright galaxies have accurate photometric redshifts, much more accurate than the faint ones. Particularly, many catastrophic outliers disappear with the shallow integrations. This is because some bands are able to distinguish the real redshift of the galaxy and the catastrophic error, for instance as we have already mentioned the u band can help remove low redshift galaxies which are assigned a high photometric redshift. However, a high signal to noise is needed which is available for the bright galaxies and not for the faint ones.

We have taken the data used in Fig.8 and plotted the scatter as a function of redshift in Fig.9. As we can see there is a definite trend of having a lower scatter if the sample taken has a high signal to noise ratio for the magnitude estimates. We can follow from the lower curve to the curve situated on the top how increasing the depth of a catalogue with the same data may produce more galaxies with photometric redshift of worst quality.

3.5 Impact of the training set depth

We have assumed so far that the training set used to train the neural networks is totally representative of the testing set we use to produce the 2D probability densities and scatter plots to assess the photometric redshift accuracies. For most cases this requires a training set which is complete down to a magnitude limit of 25. Observationally this is a hard task as spectrographs have limited spectral ranges and the features required for a redshift estimation change in observed wavelength. It should be easier to produce such a training set down to 24 or 24.5 and in the redshift range 0 to 1.4 (Le Fèvre et al. 2005).

However the faint end and high redshift range might pose some problems. One efficient way to get redshift estimates in the range 1.4 to 3 is in the blue optical and UV (Steidel et al. 1999; Lilly et al. 2006) There are many metal absorption features in this range and Lyman-Alpha comes into the optical window at $z = 1.8$. This is what currently high- z surveys are doing successfully. Another option is to have large spectroscopic redshift survey in the IR which currently does not exist but will be done with FMOS (Dalton et al. 2006) in the near future. However we have to assume this being optimistic in the case the training set is not as wealthy as we have estimated here.

We stress here that the errors which will be associated to training sets arise from two terms, one is the square root of the number of spectra N_s available in our analysis. The second is the rms sigma as a function of redshift for that group of galaxies. Weak gravitational lensing is sensitive to the error on the mean of the redshift for galaxies which is dependent on the quantity $\sigma^2(z)/N_s$. This error is complex to analyse as $\sigma(z)$ depends on the photometric bands as well as the method used for photometric redshift estimation. An analysis of this is made in Sec.5.

To assess the impact of an incomplete training on the accuracy of the photometric redshifts produced we have used training sets with a brighter magnitude cut and estimated photometric redshifts in a fainter sample. We have maintained the density of training galaxies per unit of colour volume the same in all the runs. We have chosen a cut of 25.5

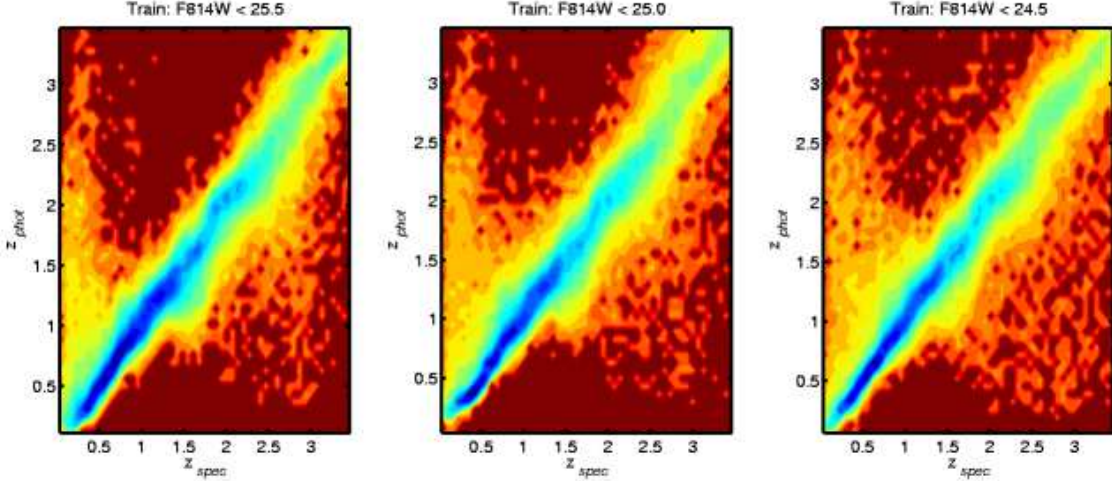


Figure 10. Effect of the training set depths in the photometric redshift quality. We have taken mocks from the survey denominated by cosmos and we have made cuts in the filter F814W at several magnitude cuts from 24.5 to 26.5 in steps of 0.5 in magnitude. We have assumed complete training sets with same number density of training galaxies per colour volume for every case shown here. As we can see the bright galaxies with high signal to noise have well constraint photometric redshifts whereas the noisy galaxies have almost unconstrained photometric redshifts. The plots are colour coded and the scale is exponential; each unit correspond to one e-fold.

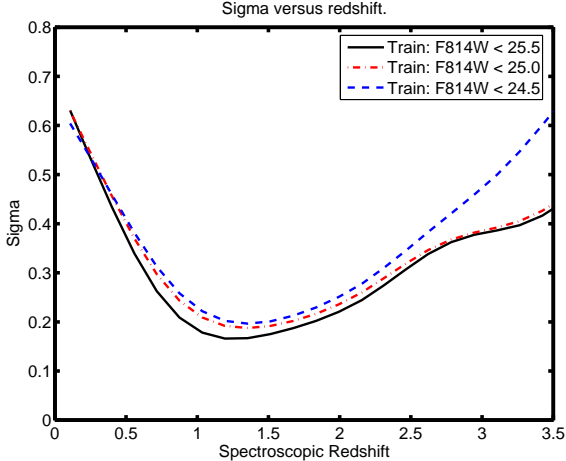


Figure 11. The scatter of $z_{phot} - z_{spec}$ as a function of redshift for samples with different training sets. Same data as in Fig.10. As we can see the sample which has been trained with an incomplete training set has worst photometric redshifts with many more outliers and larger scatter, however the decrement in accuracy is not extremely large.

in the F814W band and trained the neural networks with sets cut at 25.5, 25 and 24.5 in the same band. The probability density plots are shown in Fig.10 and the scatter as a function of redshift in Fig.11. As we can see an incomplete training produces slightly worst photometric redshifts. If we assume that we can extrapolate from the colours of the brighter objects, having only a training set complete to 0.5 magnitudes brighter degrades the photometric redshifts by about 20%. There are however, as shown in Fig.10, a much larger number of catastrophic outliers which are mainly the galaxies with no representatives in the training set.

4 COLOUR & TYPE ANALYSIS

In this section we attempt to analyse and establish which types of galaxies are producing large catastrophic outliers in the photometric redshift analysis. This is important to assess which galaxy properties are introducing the larger errors in our analysis, this would allow us to have a greater understanding of how to reduce systematic effects due to photometric redshifts and have a comprehensive understanding of how different bands can help the photometric redshift analysis.

For this purpose we choose two different catalogues to perform our colour and type analysis. We choose first a catalogue obtained from DES like exposure times however which has been cut in magnitude at $r < 24$, which is the depth of the photometry in the optical. We also choose another optical catalogue with and RIZ depth of 25 and with the specifications of the ideal optical survey we have chosen in Sec.3.2.

We plot in the centre of Fig.12 the scatter plot for the photometric redshifts as a function of the spectroscopic redshift for the first case considered, i.e. an optical DES survey with a magnitude cut at $r < 24$. From this scatter plot we have selected four regions in this $z_{phot} - z_{spec}$ plot which contain large numbers of catastrophic outliers. These regions have been selected by horizontal cuts in spectroscopic redshift at 0 to 0.35, 0.35 to 0.6, 0.65 to 0.9 and 1.6 to 2.3; the regions contain all points which have $|z_{phot} - z_{spec}| > 0.3$ on one of the sides of the $z_{phot} = z_{spec}$ curve.

We plot on the four panels above and below the scatter diagram the relative histograms of the populations within the regions selected relative to the average population of galaxies considered in the magnitude cut. This means that if the histograms are above one this galaxy type or A_v is dominant in the region selected, whereas if the histogram is below one then the population in the region is sub-dominant.

We can see that in the first region, most galaxies that are scattered towards higher photometric redshifts have a

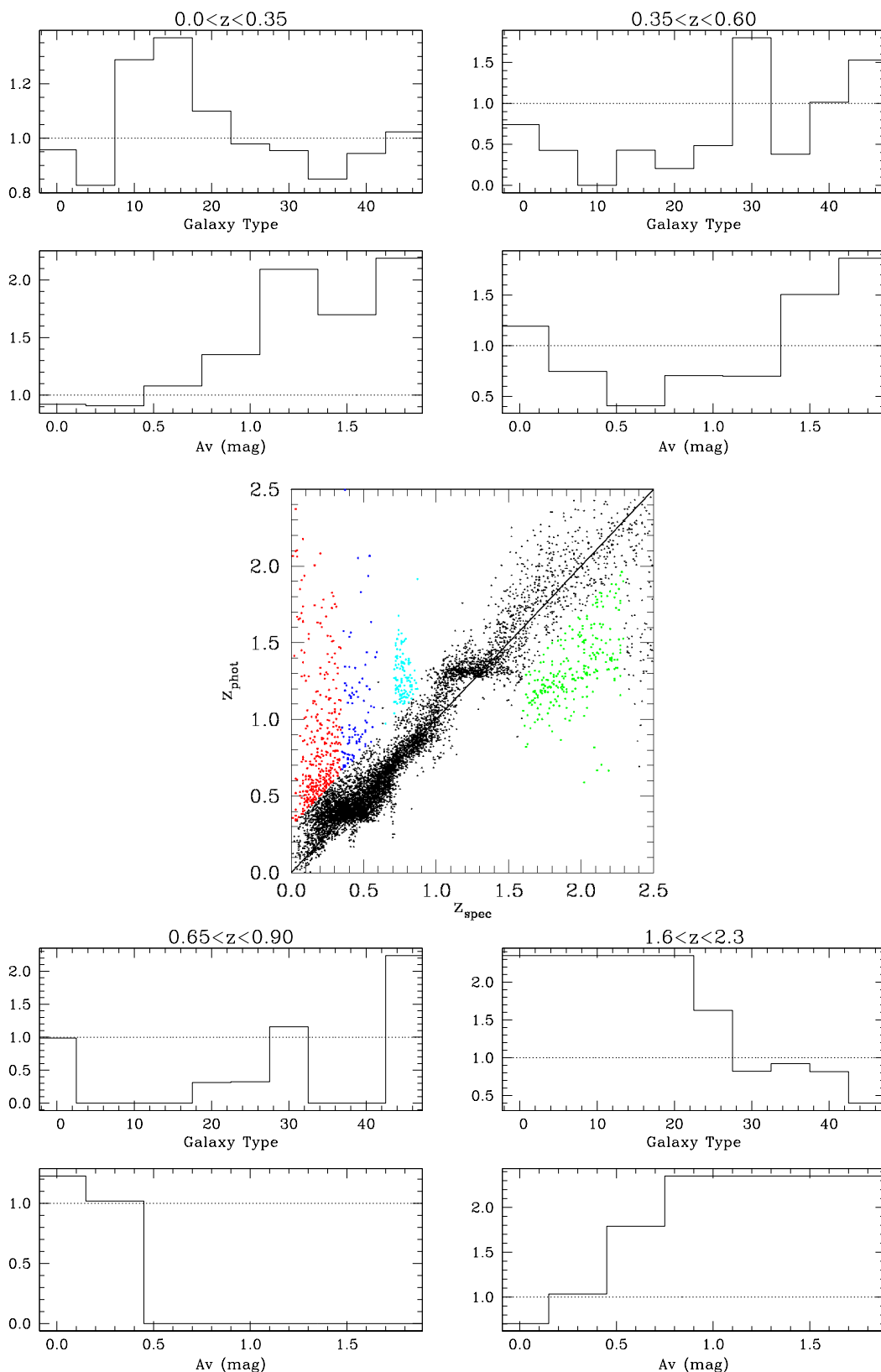


Figure 12. In the central panel the scatter plot for a DES-like optical survey cut at a magnitude limit of $r < 24$. From this scatter plot we choose four different regions dominated by catastrophic outliers. These four regions are plotted in different colours. The regions are defined by cuts in constant z_{spec} and a certain distance from the $z_{\text{spec}} = z_{\text{phot}}$ line. On the four other plots we represent the normalised histograms for the populations belonging to the regions we have chosen. We normalise the histograms to the average population on the entire sample. We can clearly see that three of the regions are dominated by highly reddened galaxies; furthermore we find that a lot of the catastrophic outliers have type of 30+ which correspond to starburst type galaxies.

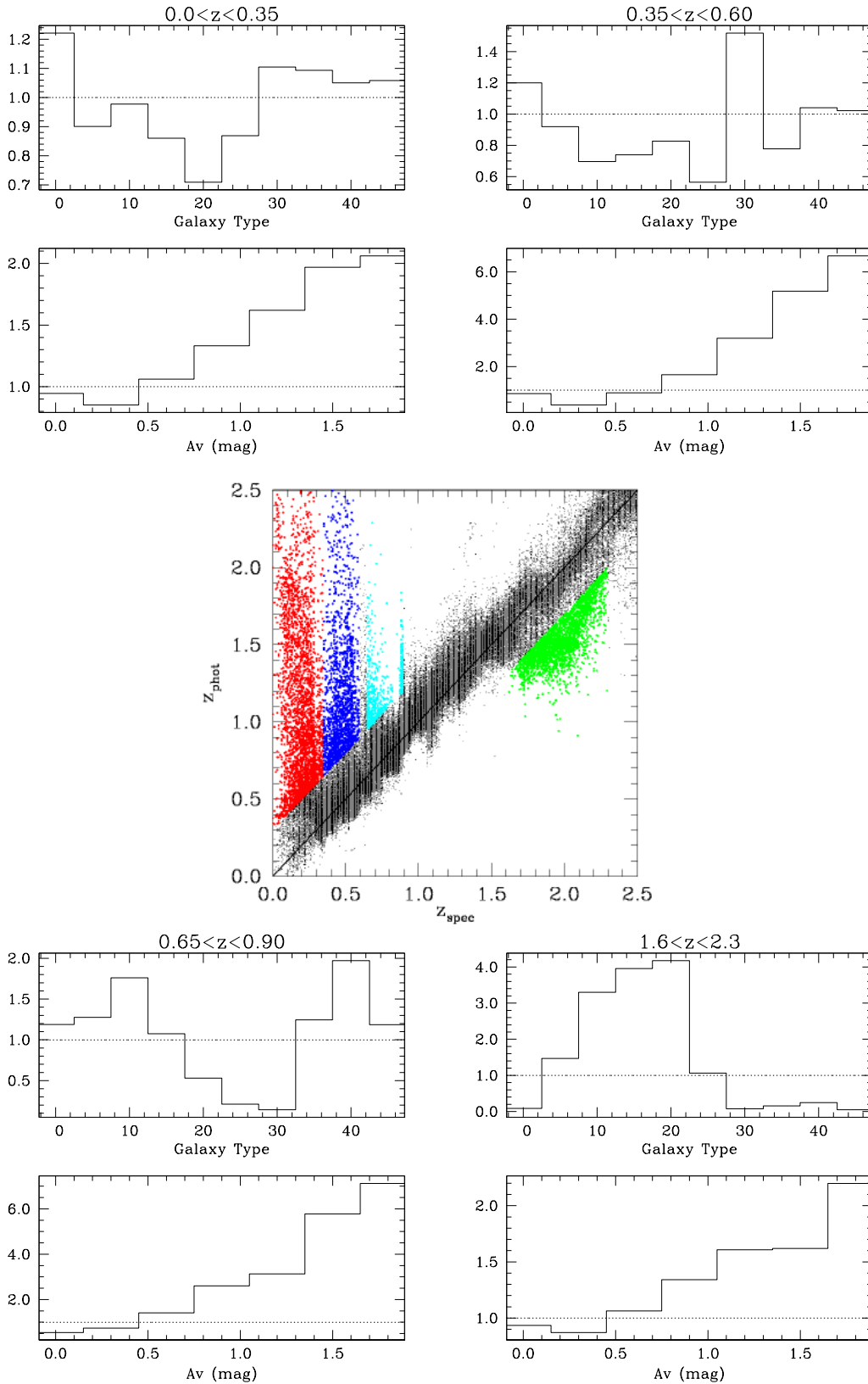


Figure 13. Mock data similar to Fig.12 but with the survey we have labelled by ideal optical survey without u band photometry. We find that basically despite the difference in the magnitude limit of the survey the regions that have a high concentration of outliers contain similar types of galaxies which are mainly reddened galaxies and/or starburst galaxies. The main difference is that in the region 1.6 to 2.3 in redshift the outliers have a low fraction of elliptical galaxies. This is due to the high exposure times in the y and z bands chosen in this mock ideal survey.

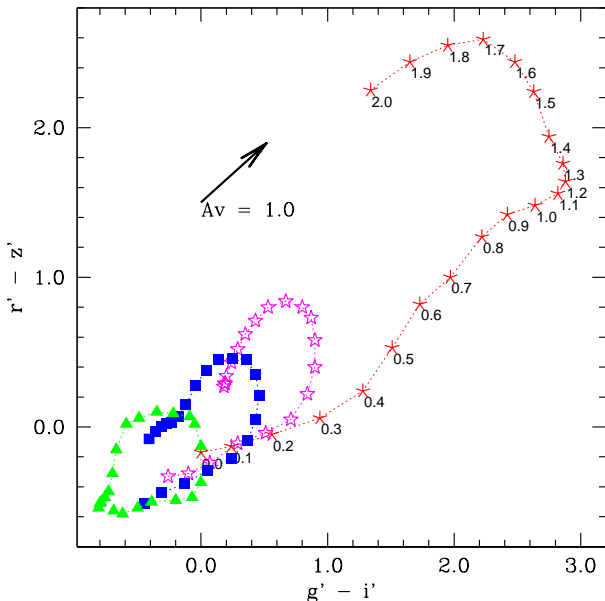


Figure 14. Colour-Colour ($g-i$ vs $r-z$) diagram of the different galaxy types with redshifts ranging from 0 to 2. The red points represent elliptical galaxies. The lowest point further to the right is the colour of an elliptical galaxy at $z = 0$, the other points are the same galaxy further along in redshift up to $z = 2.0$. Pink, dark blue and green, light blue points represent Sbc, Sdc and Irr types of galaxies. We have also plotted the vector in this plane which corresponds to the shift in colour for a reddening of $A_v = 1.0$. As we can see the shift in the colour-colour plane corresponding to redshifting the galaxy is degenerate in some cases with having a reddened galaxy. In other words a faint reddened galaxy at low redshift has very similar colours to a brighter galaxy at higher redshift with no reddening. Similarly a very high redshift galaxy which is reddened has the same colours to an intermediate redshift galaxy which is not reddened.

high A_v in our photometric catalogue. That means that galaxies which are not reddened have relatively good photometric redshifts whereas galaxies which are heavily reddened are scattered up towards high redshift. We can see from the second region chosen that the same occurs there, however this happens for different types of galaxies. The same occurs for the fourth region chosen, above a redshift of 1.6, but here the galaxies which are severely reddened are scattered towards lower redshifts. The third region we have selected is heavily populated by galaxies with types close to 50 which corresponds in our notation to very blue and young starburst galaxies which are naturally hard to get photometric redshifts for because of their relatively featureless continuum. We conclude from these graphs that the main source for catastrophic photometric redshifts for an optical survey down to $r < 24$ arises from heavily reddened galaxies as well as very blue starburst galaxies.

We have performed the same analysis with similar regions for the ‘Ideal’ survey considered. We plot similar plots in Fig.13. We can see that the results are very similar to the results obtained for a cut one magnitude fainter. The main differences are that in region four with redshift larger than 1.6 the late type galaxies with type close to zero are well constrained by the optical data given the very deep expo-

sure times in the z and y bands. Furthermore the scatter in that region is significantly lower. However the less well constrained objects have still the same properties of being either blue starburst objects or heavily reddened objects.

We can see from Fig.14 that there is a big degeneracy between redshift and reddening for some redshift ranges. We plot for different galaxy types the colour in the $r-z$ and $g-i$ plane for galaxies at different redshifts. We also plot the vector which corresponds to the average shift in colour for a reddening of $A_v = 1.0$. Clearly galaxies at low redshift which are reddened have very similar colours to galaxies at higher redshift which are not reddened. We can see with this explanation why galaxies are scattered upwards in the $z_{spec} - z_{phot}$ plane. We have used a neural network to obtain photometric redshifts; given that the training set we have chosen is representative there will be more galaxies at redshift $z \sim 1$ than at low redshift. We argue that the inclusion of IR data helps the distinction between reddened galaxies and galaxies with a low A_v given the different extinction as a function of wavelength which is low at IR bands. The case which we have chosen with an ideal + u survey also can distinguish between galaxies with a high and low A_v ; this is because at very high exposures for the u band, a detection in u would allow us to know whether the galaxy is reddened. This is because of the high extinction in the u band.

5 WEAK LENSING TOMOGRAPHY: THE DEPENDENCE OF THE DARK ENERGY PARAMETER ESTIMATION ON THE PHOTO-Z ACCURACY

5.1 A qualitative treatment of the WL-photoz cross talk

One important application of photometric redshifts is for the analysis of weak lensing tomography (Hu 1999), as e.g. in the DUNE experiment. The idea is to slice a lensing survey into photometric redshift bins and to analyse the cosmic shear for high signal-to-noise galaxy images in each photo- z bin, e.g. as discussed by Ma et al. (2006), hereafter MHH and by Amara & Refregier (2006), hereafter AR.

Specifically, we can divide the galaxy sample into photo- z bins and examine the effect on the derived cosmological parameters due to uncertainties in the photo- z s. Consider a distribution of sources selected from a photometric redshift bin which results in a more complicated (not necessarily Gaussian) distribution with respect to true (spectroscopic) redshift, with mean redshift \bar{z} and variance:

$$\mu_2 = \langle (z_{spec} - \bar{z})^2 \rangle. \quad (3)$$

Assuming Poisson statistics we can predict the variance in the mean redshift \bar{z} given N_{spec} spectroscopic redshifts associated with that photo- z bin:

$$(\delta z)^2 \equiv rms^2(\bar{z}) = \mu_2 / N_s. \quad (4)$$

We can now model crudely the uncertainty in deriving the constant Dark Energy parameter $w = P/\rho$ from WL if the only uncertainty is due to photo- z errors:

$$|(\delta w)/w| = a(\delta z)/\bar{z}. \quad (5)$$

The ‘fudge factor’ a can be estimated from detailed

modeling of the WL power spectrum. For example, if we set all other parameters to be known in the scaling relation given in Huterer et al. (2006, Eq.24) we find that $\bar{z}^{1.6} \propto |w|^{0.31}$ and hence $a = 5.2$. This value $a \approx 5$ can also be justified qualitatively by examining the sensitivity of cosmological distance and the linear growth to variations in w (Peacock & Schneider 2006).

We can now combine the last two equations to give:

$$|(\delta w)/w| = (a/\bar{z})\sqrt{\mu_2/N_s}. \quad (6)$$

For example, for a desired fractional error of 1% on w , $a = 5$, $\bar{z} = 1$ and $\mu_2 = 0.06$ (derived from our mocks and ANNz averaged over a range of proposed optical and IR surveys) we find that $N_s \approx 15,000$ spectroscopic redshifts are required for that bin, or for say 10 bins a total of 150,000 spectroscopic redshifts.

Our back-of-the-envelope calculation helps to understand the link between the Dark Energy parameters, the photometric redshift performance and the number of spectroscopic redshifts. However, being derived only for a constant w and with other cosmological parameters fixed, it somewhat underpredicts our detailed calculation below which is done for a 2-parameter equation of state and after marginalization over other parameters.

More generally Amara & Refregier (2006) have considered the way the FOM for the Dark Energy parameters (w_0, w_a) is affected by photo-z errors alongside the effect of the sky coverage and depth, the shear measurements systematic and uncertainties in the non-linear power spectrum predictions. Their scaling relations roughly agree with our detailed FOM calculations described below.

5.2 Dark Energy Figure of Merit (FOM) calculation

We summarise below the ingredients for the FOM calculation for Dark Energy parameters from weak lensing. The predicted angular power spectrum $C_{ij}(l)$ between redshift bins i and j depends on the 3-D matter power spectrum $P(k = l/r)$ and on the radial window functions $W_i(r)$ and $W_j(r)$ of bins (i, j) :

$$C_{ij}(l) = \int_0^{r_H} dr r^{-2} W_i(r) W_j(r) P(l/r; r) + \delta_{ij} \sigma_e^2 / \bar{n}_i, \quad (7)$$

where r is the comoving distance and r_H is the Universe horizon. The last term is the ‘shot noise’ due to σ_e , the intrinsic ellipticity noise for the galaxy sample, and \bar{n}_i , the total number of galaxies in the radial slice. The case $i = j$ gives the auto-correlation of bin i . The window function $W_i(r)$ depends on cosmological parameters and on the redshift distribution $p_i(z)$ of the source galaxies redshift slice, normalised such that $\bar{n}_i = \int dz p_i(z)$ is the total number of galaxies in the slice and the integral is over the slice’s radial boundaries. For a comprehensive list of detailed equations in weak-lensing correlations we refer the reader to (Bridle & King 2007).

Ideally, we would like to know the $p_i(z)$ exactly from a spectroscopic survey, where the redshift is derived from the spectrum of each galaxy. In reality, deep wide field surveys, such as DUNE, will only provide us with multi-band imaging data which will allow us to derive photometric redshifts

	DES	Pan-4	LSST	Ideal	Ideal + u
RIZ	72	80	116	136	164
RIZ + IR	120	132	156	168	168

Table 3. The FOM for the survey configurations we consider with and without IR data. The FOM results are for a lensing survey only and do not include any other prior such as CMB.

based on templates and/or spectroscopic training sets. We can relate the probabilities for the true redshift z_{spec} and the photometric redshift z_{phot} by the Bayesian rule of conditional probability:

$$p(z_{spec}, z_{phot}) = p(z_{spec}|z_{phot})p(z_{phot}) = p(z_{phot}|z_{spec})p(z_{spec}) \quad (8)$$

Consider now a sharp cut in a photo-z bin i , i.e. we select only those galaxies in the range $z_{phot}(i) < z_{phot} < z_{phot}(i+1)$. We can write the probability for the true redshift distribution resulting from the photo-z slice as:

$$p_i(z_{spec}) = \int_{z_{phot}(i)}^{z_{phot}(i+1)} p(z_{phot}, z_{spec}) dz_{phot} \quad (9)$$

Typically $p_i(z_{spec})$ would have a wide spread, *not* in the form a Gaussian, as a-symmetric tails are present due the photo-z catastrophic errors.

We have now two options. One is to parameterise $p_i(z_{spec})$ directly based from the projection of the photo-z scatter diagram $p_i(z_{spec}, z_{phot})$, derived based on a spectroscopic training set or mock catalogues. The second option is to model it using eq. (8):

$$p_i(z_{spec}) = \int_{z_{phot}(i)}^{z_{phot}(i+1)} p(z_{spec}) p(z_{phot}|z_{spec}) dz_{phot}, \quad (10)$$

where $p(z_{spec})$ is the overall galaxy redshift distribution and $p(z_{phot}|z_{spec})$ can be modelled, somewhat ad-hoc, as a Gaussian (e.g. MHH, AR).

Here we prefer the first option, i.e. we use the actual distributions of spectroscopic redshifts coming out of the simulations for the analysis.

The uncertainties in the shapes of the probability distribution function also have to be taken into account, due to the finite number, N_s , of the spectroscopic redshifts per bin in the training set. We have assumed an uncertainty on the mean and on the variance of the distributions we have from the photo-z simulations for each redshift shell in our analysis. As explained in the previous sub-section, from Poisson statistic we can predict the variance in the mean redshift of the bin:

$$rms^2(\bar{z}) = \mu_2(z_{spec})/N_s \quad (11)$$

where $\mu_k(z_{spec}) = \langle (z_{spec} - \bar{z})^k \rangle$ for a given photometric redshift bin. Similarly for the variance in the variance

$$rms^2(\mu_2) = \frac{N_s - 1}{N_s^3} [(N_s - 1)\mu_4 - (N_s - 3)\mu_2^2] \simeq \frac{\mu_4 - \mu_2^2}{N_s}. \quad (12)$$

One can marginalise over both these uncertainties. The dependence on the number of spectroscopic redshifts is really an indirect expression of the the scatter in \bar{z} and in μ_2 .

The Dark Energy equation of state is commonly written as: $w(a) = w_0 + (1 - a)w_a$. One can also define a_p , the pivot value at which the uncertainty in $w(a)$ is the minimal.

Accordingly we define $w_p = w_0 + (1 - a_p)w_a$. Armed with this parameterisation we can now apply the Fisher matrix formalism. We define FOM⁴ as:

$$\text{FOM} = \frac{1}{(\det F_{ij}^{-1})^{1/2}} = \frac{1}{\delta w_p \delta w_a} \quad (13)$$

where i and j denote the elements of the covariance matrix (F^{-1}) that contain the equation of state parameters (w_p, w_a) and δw_p and δw_a are the 68% errors on w_p and w_a .

In our Fisher matrix analysis we vary the following cosmological parameters: the dark matter content Ω_m , the dark energy parameters w_0, w_a , the Hubble constant divided by 100 h , the amplitude of fluctuations at $z = 0$ σ_8 , the baryonic matter content Ω_b and the scalar index of the primordial spectrum n where the fiducial values are 0.3, -0.95, 0.0, 0.7, 0.8, 0.045 and 1.0 respectively. We assume spacial flatness. As we have already stated we have also assumed that there is an uncertainty over the mean and variance for each of the redshift bins independently. Hence we have two extra nuisance parameters that we will marginalise over for each photometric redshift bin.

When performing a lensing measurements, cuts are made on the detected galaxies. The two most significant cuts are in flux, where galaxies below a certain magnitude threshold are not used, and a size cut where small galaxies are rejected because their shape is hard to measure. In this work we have not included a size cut since this would require detailed image simulations which is beyond the scope of this paper. However the effect of this cut is important since this will remove high redshift galaxies from our sample. To mimic the effect of these cuts we randomly sample the galaxies in our mock and apply a selection so that our galaxy population has a more realistic PDF. Specifically we impose a distribution ($P(z) = z^2 \exp(-(z/z_0)^{1.5})$), where z_0 is set by the median redshift of the galaxies ($z_0 = z_m/1.412$), which we assume to be $z_m = 0.9$.

We have performed all the analysis with five photometric redshift bins and also checked that having more photometric redshift bins did not improve considerably on the FOM. We have chosen the photometric redshift bins so that the number of galaxies in each bin was the same. The total number of galaxies considered was 35 gal/arcmin² and we have considered a survey covering 20000 deg².

5.3 FOM results

We now investigate the role of the IR filters in the FOM prediction. We can clearly see that the role of the IR filter depends on the quality of the optical data available. We found before that the scatter plots for the photo- z benefited significantly by the inclusion of IR data. Here we find that if we have poor optical data with depth similar or shallower than the target depth of 25 in the RIZ filter, then the IR bands can improve the FOM by a factor of 1.7. However if the optical data available is deeper than the target depth of 25

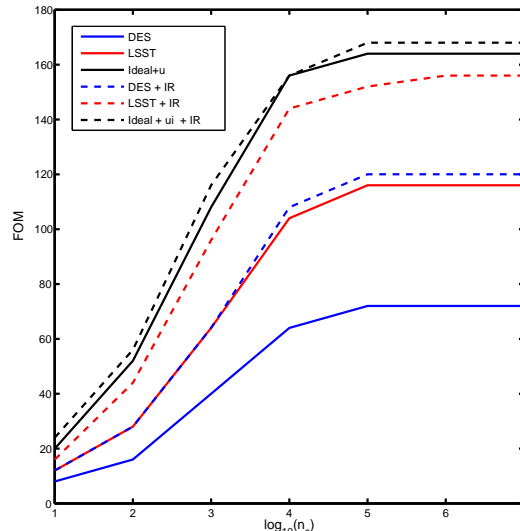


Figure 15. The FOM as a function of the number of spectroscopic redshifts (per bin) used to calibrate the photometric results. We can see that the FOM began to level off at 10^4 and having more than 10^5 spectroscopic redshifts does not increase the FOM thus meaning that the photo- z are well enough calibrated. We conclude that for a DUNE-like survey we will need around 10^5 objects in each redshift bin (here we assumed 5 bins) to calibrate the photometric redshift. Around 10^4 objects might be sufficient, however the use of Eqn.11 does not take account of outliers or the non-Gaussianity of the distribution and a number closer to 10^5 will be necessary. Furthermore there redshifts must be representative of the sample and therefore most of them should be of galaxies in the faint end of the catalogue, i.e. fainter than RIZ of 24.

in the RIZ filter, especially in the z and y bands than this improvement is reduced to 1.3^5 and if very deep u band data are available then the improvement is minimal for the purposes of Dark Energy determination.

All the numbers above assume an infinite number of spectroscopic redshifts are available to calibrate the photometric data. In practice only a finite number is necessary in order to calibrate the data well enough so that there is no degradation of the FOM. In order to assess this we have performed Fisher matrix calculations where we have prior knowledge given by N_s , the number of spectroscopic galaxies. We show the results in Fig.15. As we can see if we have around 10^5 galaxies in each of the photometric redshift bins that we have assumed we have very little degradation of the FOM. We therefore conclude that we will require that many spectroscopic redshifts to calibrate the photometric sample well enough. Obtaining this many spectra is not a daunting process. However, we emphasise that most of these spectroscopic redshifts should be of galaxies in the faint end of the sample which will be the most numerous. A sample of 10^5 galaxies at high brightness would not be suitable. As we dis-

⁴ The Dark Energy Task Force report (Albrecht et al. 2006) defined The Figure of Merit slightly differently as the reciprocal area in the $w_0 - w_a$ plane that encloses 95% CL region. It differs to our FOM by a constant factor.

⁵ In comparison the DEFT report (Albrecht et al. 2006) suggests that a new generation of surveys should improve the FOM by a factor of 3. Here the improvements with IR are a factor of 1.3 to 1.7 within the same survey generation.

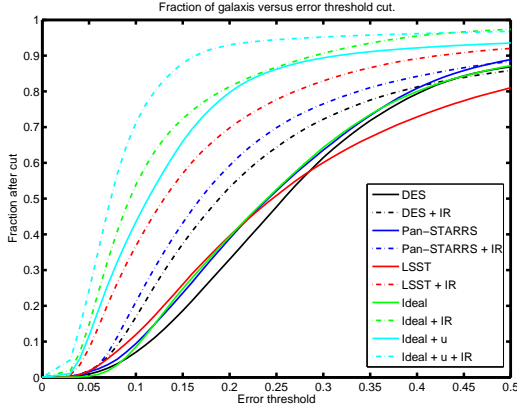


Figure 16. The fraction of galaxies removed from each of the surveys considered if we apply a cut in the photometric redshift error. As we can see the inclusion of the IR bands increases significantly the accuracy of the error determination in our analysis. We also note that among the mock sets with simulated optical data only, the one with u band data is also reliable in obtaining a reliable error estimate. Furthermore as it is argued it is possible to clean photo-z catalogues removing outliers without decreasing significantly the FOM for Dark Energy parameters.

cussed in Sec.3.5 this spectroscopic sample is currently not available, however, with IR surveys probing galaxies at a redshift of 2 combined with surveys such as zCOSMOS the prospects of having such a sample in the next decade is not unfeasible. However there is need for more detailed study to assess whether this sample will be adequate in terms of completeness so that it will be able to calibrate photometric redshifts.

5.4 Other considerations: systematic effects.

We have assessed the impact on the statistical errors that different photometric redshift distributions would have constraining the Dark Energy parameters. In a weak lensing survey, however, there will be further systematic barriers which would not allow this statistical limit to be reached.

One of the important effects that will have to be removed or modelled and fitted for is the effect of intrinsic alignments for close-by galaxies. The intrinsic-intrinsic (II) power spectrum introduced by galaxy intrinsic alignments can be written as

$$C_{ij}^I(l) = \int_0^{r_H} dr r^{-2} p_i(r) p_j(r) P_{II}(l/r; r), \quad (14)$$

where p_i is the redshift distribution for the galaxies in bin i and P_{II} is the intrinsic alignment power spectrum. We can see that if p_i and p_j are independent the contamination of the II term is minimal. Therefore weak lensing surveys would require a low overlap of galaxies between different bins. Several ideas have been proposed recently to improve the performance of the WL analysis. Jain et al. (2006) suggested a ‘colour tomography’ to bin the galaxy data in colour space where galaxies have small overlap in the p_i , rather than to generate a photo-z catalogue and then bin it.

It is beyond the scope of this paper to do a complete analysis of how these systematic effects will hinder the

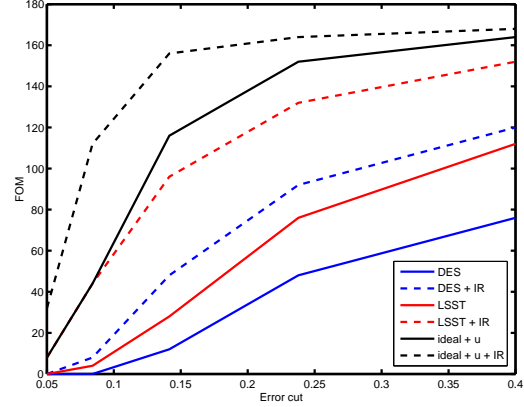


Figure 17. The FOM as a function of the photometric redshift error cut. We can see that for deeper surveys. As we can see if we have a survey with deep IR bands or a survey with deep u band photometry than performing a cut to remove outliers does not decrease the FOM significantly. This is clearly a function of how deep the optical survey is. We can see in Fig.5 the quantity of outliers left on the mocks with a cut of 0.3.

FOM for the Dark Energy parameters we refer the reader to (Bridle & King 2007) for a more detailed analysis of this. However we have assessed to what extent a detailed analysis of photometric redshift errors would help improve the contamination of the II term in weak lensing. We have run Fisher matrices for catalogues which were cut in increasing redshift error. That is to say that galaxies that are found to have high error estimates are removed from the sample, this can be seen in Fig.16. We plot the fraction of galaxies left in this sample. Consequentially there are less systematic errors as there are fewer outliers in the sample. We can see from Fig.5 how this affects the number of outliers in the photo-z analysis for a given cut in the estimated error.

We plot in Fig.17 how the FOM is decreased by a photo-z error cut for some of the surveys considered. We can see clearly that some surveys can have a large cut in the photometric redshift error and their FOM remains almost unchanged. This clearly means that we will be removing systematic errors due to the overlap of the photometric redshift bins but not hitting the FOM by removing galaxies which introduce relevant information in the determination of Dark Energy. Furthermore, if there is the need to model a galaxy-intrinsic (GI) alignment contribution to the cosmic shear signal, this will be more reliable if we obtain a sample with only the reliable photometric redshifts and which does not decrease the FOM significantly compared to the full sample.

6 CONCLUSIONS

In this work we have looked at the role of optical and near-IR photometry in the context of weak lensing tomography. In particular we have quantified how the Figure of Merit for Dark Energy parameters is affected by the choice of filters and observing conditions. We have generated catalogues from a range of proposed surveys. For fixed mock simulations and fixed photo-z method (ANNz) we explored the photo-z accuracy and systematics by varying the set of filters and

the magnitude limit of the surveys. The aim of this was to compare the role of bands and to reduce biases given that different mocks and photo-z methods may give different answers.

From the photometry, we find that there is an interplay between the choice of filters (in particular the J, H and the u), the depth (i.e. magnitude limit), and the removal of outliers based on the photo-z errors. We find that if we are to get IR data from space the improvements are greatly dependent on the quality of the ground data available. For surveys that go down to the same magnitude limit as the lensing survey in the RIZ band the improvements that the J and H bands bring are great. However, if we have ground based photometry, particularly in the z and y bands, the improvements due to IR data becomes smaller. There is a trade-off between the u and the IR, meaning that the u band, provided it is deep enough, can play a similar role as the IR data.

In summary, our main conclusions are:

- The addition of J+H to griz+RIZ dramatically reduces the scatter in individual photo-z, in particular for the shallow griz surveys.
- The u band filter is effective in removing outliers and can play a similar role as the IR filters but only if the RIZ depth is significantly larger than the depth of the lensing survey chosen.
- The results presented here depend on galaxy formation scenarios which are encoded into the mock catalogues. The main source for catastrophic photometric redshifts for an optical survey arises from heavily reddened galaxies as well as very blue starburst galaxies. It is hard to distinguish between a higher redshift galaxy and a lower redshift reddened galaxy with optical colours only below $z \sim 1.2$. The opposite is true above $z \sim 1.7$. The inclusion of u band data or IR data breaks this degeneracy.
- Our derived Figure of Merit $FOM = [\delta w_p \delta w_a]^{-1} \sim 160$ can be obtained with a realistic mock catalogue solely with weak lensing data. This would be a significant increase over current estimates and also the next generation of surveys. For comparison a current estimated of the error on w is $[\delta w_p]^{-1} \sim 10$.
- Given an ambitious ground based surveys such as the LSST + IR bands from space, only marginal improvement in FOM (see Table 3) can be achieved by increased the photometric accuracy of the visible bands. Since increasing the accuracy of the visible bands will likely require deep space lensed data, the extra cost of this is difficult to justify.
- The FOM improvement if we add IR data depends on the quality of the ground based optical data. The FOM is increased by a factor ranging from 1.7 down to 1.3 for realistic mock surveys.
- The required number of spectroscopic redshifts needed depends on the number of galaxies to train a neural network and also the quantity of galaxies needed to calibrate the photometric redshifts. We argue that a value around 10^5 in each redshift bin will be necessary for weak lensing studies from future space based missions.
- The ‘cleaning’ of outliers is effective. There is a trade-off between reducing the photo-z error by removing galaxies, but increasing the shot noise. It is possible to clean a photo-z catalogue without decreasing the FOM significantly. We conclude that this is an effective way to decrease systematic

effects from a weak lensing survey and is an alternative to colour tomography.

The general conclusion from our study is that combining weak lensing measurements from space and photometric redshifts from optical ground-based data is indeed a very attractive way to constrain Dark Energy properties. Furthermore, the use of IR from space can significantly improve the accuracy of Dark Energy measurements by 30-70 percent.

ACKNOWLEDGEMENTS.

We thank Manda Banerji, Sarah Bridle, Huan Lin, Alex Refregier, the DES and DUNE weak-lensing and photometric redshift working groups and the COSMOS team for useful discussions. OL acknowledges a PPARC Senior Research Fellowship. This research was carried out in part at the Jet Propulsion Laboratory, California Institute of Technology, under a contract with the National Aeronautics and Space Administration and funded through the internal Research and Technology Development program.

REFERENCES

- Albrecht et al. 2006, astro-ph/0609591
Aldering et al. 2004, Supernova / Acceleration Probe: A Satellite Experiment to Study the Nature of the Dark Energy
Amara A., Refregier A., 2006, astro-ph/0610127
Bishop C. M., 1995, Neural Networks for Pattern Recognition (New York: Oxford Univ. Press)
Blake C. A., Abdalla F. B., Bridle S. L., Rawlings S., 2004, New Astronomy Review, 48, 1063
Blake C. A., Glazebrook K., 2003, ApJ, 594, 665
Bridle S., Abdalla F. B., 2007, ApJ Lett., 655, L1
Bridle S., King L., 2007, astro-ph/0705.0166
Budavári et al. 1999, in Weymann R., Storrie-Lombardi L., Sawicki M., Brunner R., eds, ASP Conf. Ser. 191: Photometric Redshifts and the Detection of High Redshift Galaxies Creating Spectral Templates from Multi-color Redshift Surveys. pp 19–
Calzetti D., 1997, AJ, 113, 162
Coleman G. D., Wu C.-C., Weedman D. W., 1980, ApJS, 43, 393
Collister A. A., Lahav O., 2004, PASP, 116, 345
Cowie L. L., Barger A. J., Hu E. M., Capak P., Songaila A., 2004, AJ, 127, 3137
Csabai et al. 2003, AJ, 125, 580
Dalton G. B., Lewis I. J., Bonfield D. G., Holmes A. R., Brooks C. B., Lee H., Tosh I. A. J., Froud T. R., Patel M., Dipper N. A., Blackburn C., 2006, in Ground-based and Airborne Instrumentation for Astronomy. Edited by McLean, Ian S.; Iye, Masanori. Proceedings of the SPIE, Volume 6269, pp. 62694A (2006). Vol. 6269 of Presented at the Society of Photo-Optical Instrumentation Engineers (SPIE) Conference, The UK FMOS spectrograph
Heymans C., Heavens A., 2003, MNRAS, 339, 711
Heymans C., White M., Heavens A., Vale C., van Waerbeke L., 2006, MNRAS, 371, 750
Hirata C. M., Seljak U., 2004, Phys. Rev. D, 70, 063526
Hu W., 1999, ApJ Lett., 522, L21

- Hu W., Haiman Z., 2003, *Phys. Rev. D*, 68, 063004
- Huterer D., Takada M., Bernstein G., Jain B., 2006, *MNRAS*, 366, 101
- Jain B., Connolly A., Takada M., 2006, [astro-ph/0609338](#)
- King L., Schneider P., 2002, *A&A*, 396, 411
- King L. J., Schneider P., 2003, *A&A*, 398, 23
- Kinney A. L., Calzetti D., Bohlin R. C., McQuade K., Storchi-Bergmann T., Schmitt H. R., 1996, *ApJ*, 467, 38
- Le Fèvre et al. 2005, *A&A*, 439, 845
- Lilly et al. 2006, [astro-ph/0612291](#)
- Ma Z., Hu W., Huterer D., 2006, *ApJ*, 636, 21
- Madau P., 1995, *ApJ*, 441, 18
- Massey et al. 2006, [astro-ph/0608643](#)
- Peacock J., Schneider P., 2006, *The Messenger*, 125, 48
- Perlmutter et al. 1999, *ApJ*, 517, 565
- Réfrégier et al. 2006, in *Space Telescopes and Instrumentation I: Optical, Infrared, and Millimeter*. Edited by Mather, John C.; MacEwen, Howard A.; de Graauw, Mattheus W. M. *Proceedings of the SPIE*, Volume 6265, pp. 62651Y (2006). DUNE: the Dark Universe Explorer
- Riess et al. 1998, *AJ*, 116, 1009
- Seo H.-J., Eisenstein D. J., 2003, *ApJ*, 598, 720
- Steidel C. C., Adelberger K. L., Giavalisco M., Dickinson M., Pettini M., 1999, *ApJ*, 519, 1
- Turner M. S., White M., 1997, *Phys. Rev. D*, 56, 4439
- Wirth et al. 2004, *AJ*, 127, 3121